Single-Particle Excitations in Quasi-Zero- and Quasi-One-Dimensional Electron Systems

R. Strenz, U. Bockelmann, F. Hirler, G. Abstreiter, G. Böhm, and G. Weimann
Walter Schottky Institut, Technische Universität München, D-85748 Garching, Germany
(Received 19 July 1994)

Resonant inelastic light scattering is used to probe electronic excitations in shallow etched GaAs/AlGaAs quantum dots and wires. In both types of structures, intersubband excitations are observed in depolarized scattering geometries. They show significant blueshift with decreasing confinement length. In dot structures these transitions appear as dispersionless, whereas in wires they show strong broadening and an intensity dip at the energetic center of the excitation with increasing wave vector parallel to the wires, as expected for single-particle excitations. Their line shape correlates with the linear wave vector dispersion of additionally observed intrasubband excitations.

PACS numbers: 71.50.+t, 78.30.Fs

The study of electronic excitations in semiconductor heterostructures of reduced dimensionalities has attracted an enormous amount of research activity in recent years. Resonant inelastic light scattering by electronic excitations has been shown to be a powerful characterization method. It allows an investigation of the wave vector dispersion as well as the distinction between charge density (CDE), spin density (SDE), and single-particle excitations (SPE) by means of polarization selection rules [1,2]. Apart from extensive studies on two-dimensional electron systems much work has already been done on one-dimensional electron systems in the extreme quantum limit. One-dimensional intrasubband SDE, SPE, and CDE as well as intersubband CDE in a sample with only two occupied subbands were investigated by Goñi *et al.* [3]. Recently, the first observation of intersubband SDE was reported [4,5]. Inelastic light scattering in systems with several occupied subbands has been performed by Egeler *et al.* [6]. They studied the anisotropic wave vector dispersion of confined plasmons. Apart from this collective excitation, SPE are a dominant feature of the excitation spectrum in this confinement regime [7], where exchange-correlation contributions to the electron-electron interaction are expected to be very small [8,9]. Intersubband excitations in quasi-one-dimensional systems have been observed by Weiner *et al.* [10]. However, to our knowledge there have been no investigations of the wave vector dispersion of SPE in quasi-one-dimensional systems with several occupied subbands nor any publications on inelastic light scattering by electronic excitations in zero-dimensional systems at all.

In this Letter, we report on Raman scattering by SPE in quasi-zero- and quasi-one-dimensional systems. We observe up to three intersubband peaks in depolarized scattering geometries which show a clear blueshift with decreasing lateral confinement length. Nondispersive behavior as well as strong dependence of the scattering intensities on the wave vector component in the direction of confinement have been verified in all dot and wire samples. With increasing wave vector component parallel to the wire we find a strong broadening and an intensity dip emerging in the center of the intersubband peak. The line shape correlates with the linear wave vector dispersion of additionally observed intrasubband excitations proving the single-particle character of the excitations. The intersubband modes reflect the lateral quantization of the single-particle states.

We use holographic lithography and shallow wet chemical etching to structure n-type modulation doped GaAs/AlGaAs single-quantum-well (SQW) samples laterally. The patterning of the samples leads to a lateral type II superlattice. This method is known to produce potential modulations up to 50 meV. Sample preparation and luminescence properties of these systems are described in more detail in [11,12]. The electron density and mobility of the unstructured 80 Å wide SQW obtained from magnetotransport measurements after illumination at $T = 380$ mK are 10.8×10^{11} cm^{-2} and 1.1×10^5 cm^2/V s, respectively. The SQW is grown on a short period GaAs/AlAs superlattice and is located 360 Å below the sample surface. The light scattering experiments are performed in conventional backscattering geometry with the samples mounted in a continuous flow He cryostat at $T = 5$ K. We use a dye laser for resonant excitation in the range of the second allowed heavy-hole–electron transition of the SQW and a 0.5 m triple spectrometer with a liquid nitrogen cooled charge coupled device camera for multichannel detection. Typical excitation power densities are in the range of 50 W cm^{-2}. Nonzero in-plane wave vector transfer $q = 4\pi \sin \alpha / \lambda$ is achieved by tilting the sample normal by an angle α with respect to the linearly polarized incident laser beam of wavelength λ [1].

Figure 1 shows depolarized light scattering spectra of dot samples for different geometrical dot sizes and wave vectors. CDE do not lead to inelastic light scattering in this configuration. The lowest spectrum displays the reference measurement of the as-grown two-dimensional structure, where we observe an intrasubband SPE with linear wave vector dispersion. The maximum of the scattering intensity is close to $\hbar q v_F$, with v_F representing the Fermi velocity of the lowest subband. The line shape of

 0031-9007/94/73(22)/3022(4)$06.00 © 1994 The American Physical Society

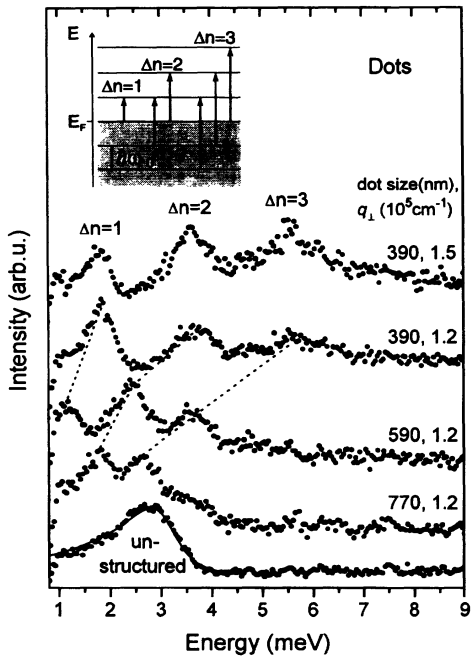

FIG. 1. Depolarized light scattering by interlevel excitations in quantum dots. The two parameters at each spectrum denote the geometrical dot size and wave vector. The lowest spectrum shows the reference measurement of the as-grown sample and a line shape fit (continuous line). All contributing transitions are schematically shown in the inset.

SPE reflects the transition density of states which can be described by the imaginary part of the corresponding electronic polarizability [1]. The continuous line is obtained from a line shape fit, using the Lindhard-Mermin expression for the 2D intrasubband polarizability [13], which leads to electron density, single-particle scattering time, and a carrier temperature of 10.8×10^{11} cm^{-2}, 1.3 ps, and 10 K, respectively. Going from the bottom to the top, the next three spectra stem from dot samples with decreasing geometrical dot size. The size of the nearly quadratically shaped dots is deduced from atomic force microscopic (AFM) investigations. The sample with the largest dots shows structure with an envelope resembling the line shape of the two-dimensional intrasubband excitation. With decreasing dot size these structures develop into nearly equidistantly separated peaks showing a significant blueshift. The energetic splitting of the modes is 1.9 meV in the smallest sample of Fig. 1, which is in the range of the expected single-particle level spacing in such dot structures. The topmost two spectra are from the same sample but with different wave vector transfer and illustrate the dispersionless behavior of all modes. We assign them to interlevel transitions within the dots as indicated by the inset of Fig. 1. These excitations might be redshifted with respect to SPE by final state effects. However, in systems with several occupied subbands this effect is expected to be very small [8,9]. Therefore we assume these excitations to reflect the single-particle level spacing at the Fermi energy. The scattering intensities of all modes increase systematically with increasing wave vector transfer. This behavior is very similar to quantum wires and will be discussed later. A slight anisotropy of the scattering intensities is observed when turning the direction of the lateral wave vector transfer from the [110] to the [100] direction. This reflects the anisotropic geometrical shape of the dots.

We now compare our results on quantum dots with light scattering data obtained from quantum wires. Figure 2 shows depolarized Raman spectra of a wire sample with 600 nm period length and 170 nm geometrical wire width. The sample is mounted in standing wave geometry, i.e., transferred momentum perpendicular to the wire direction. In this configuration we qualitatively expect a similar behavior as for quantum dots. With increasing momentum transfer perpendicular to the wire, a strong gain in intensity of all modes occurs. This is expected for SPE described by the noninteracting polarizability function [14,15]

$$\chi_{nm}(z,\mathbf{q}) \propto \int_k dk \, \frac{f(E_n(k)) - f(E_m(k+q_\parallel))}{E_m(k+q_\parallel) - E_n(k) - \hbar z} \times |\langle m|\exp(iq_\perp x)|n\rangle|^2. \quad (1)$$

$f(E)$, $E(k)$, $q_\parallel$, $q_\perp$, z, $|m\rangle$, and $|n\rangle$ denote the Fermi distribution function, the free particle wave vector dispersion, the wave vector transfer parallel and perpendicular to the wire, the complex frequency of the excitation, and the one-dimensional single-particle states of the involved subbands, respectively. For vanishing momentum transfer $q_\perp \to 0$ only the even $\Delta n = 2$ transitions are clearly observed. This is due to parity conservation which should hold for a two-photon process like Raman scattering in the case of a symmetric wire potential. We deduce a lateral subband spacing of approximately 3.3 meV in this sample, which is in agreement with magnetotransport measurements. From magnetic depopulation of the one-dimensional subbands [16] we obtain a subband spacing of about 3.5 meV assuming a parabolic potential shape. In contrast to quantum dots, where at $T = 0$ K, only j different interlevel transitions across the Fermi energy contribute to the $\Delta n = j$ interlevel peak ($j = 1,2,\ldots$) in the light scattering spectra, in quantum wires all occupied subbands act as starting levels for intersubband transitions. All these transitions contribute to the scattering intensity of the corresponding intersubband peak, as is schematically shown in the inset of Fig. 2 for transitions with zero wave vector parallel to the wire. As we observe clearly separated and nearly equidistantly spaced intersubband modes we conclude that the confining potential must be close to a harmonic oscillator potential. The observed linewidth of the peaks in this scattering geometry is essentially due to inhomogeneous broadening.

We have also studied the wave vector dispersion parallel to the wire. Figure 3 shows depolarized light scattering spectra with the wire sample mounted in plane wave geometry for different wave vectors $q_\parallel$. In this configuration, the wave vector transfer is parallel to the wire,

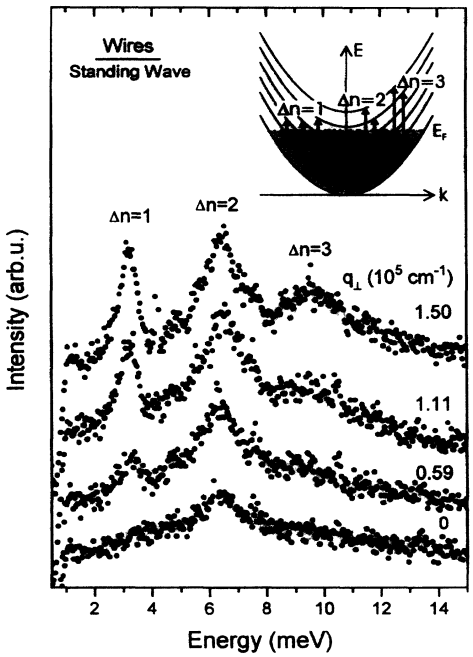

FIG. 2. Depolarized light scattering spectra of a wire sample mounted in standing wave geometry for different wave vectors $q_\perp$. The inset schematically shows intersubband excitations of different orders for $q_\parallel = 0$.

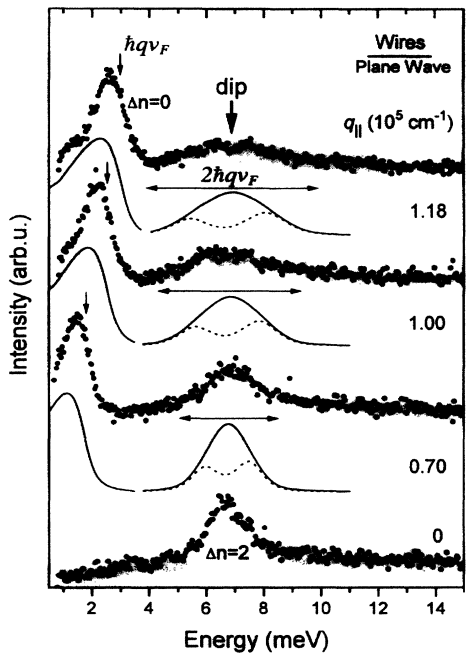

FIG. 3. Depolarized light scattering spectra of the wire sample mounted in plane wave geometry for different wave vectors $q_\parallel$. The continuous lines show calculated spectra of intrasubband and $\Delta n = 2$ intersubband excitations obtained from a harmonic oscillator model. The dashed lines show the intersubband line shape if transitions into empty levels are neglected.

and two different excitations can be observed. The mode smaller in energy is only observable for nonzero wave vector transfer and reveals a linear wave vector dispersion. The peak at 6.7 meV stems from $\Delta n = 2$ intersubband transitions. Equation (1) shows that these transitions can only occur for nonzero wave vector components perpendicular to the wire. Grating coupler effects of the etched sample surface as well as the finite numerical aperture of the collecting lens system can induce intersubband transitions even in plane wave scattering geometry. Looking at the wave vector dispersion of the intersubband peak we observe nondispersive behavior and strong broadening. For large wave vectors an intensity dip at the energetic center of the peak emerges.

Both transitions can be understood in terms of a superposition of different single-particle excitations in the system. Figure 4 illustrates the different types of one-dimensional transitions for $T = 0$ K in the absence of broadening. For intrasubband excitations each subband contributes a rectangular-shaped peak centered at $\hbar q v_F$, with v_F denoting the Fermi velocity of the subband. Finite carrier temperature and scattering time lead to broadening and a slight redshift of the peak. Assuming a constant subband spacing of 3.35 meV, solving Eq. (1) for finite temperature $T = 5$ K, taking into account a finite single-particle scattering time $\tau = 1.65$ ps by the Lindhard-Mermin expression [13], and finally summing up the intrasubband contributions of all subbands leads to the line shape shown in Fig. 3 at the left-hand side (solid line). We deduce 31 meV for the Fermi energy of the lowest subband in this system and therefore can roughly estimate ten occupied subbands. This value is in good agreement with the carrier density we obtain from confined plasmon excitations observed in polarized scattering geometry as described in [12].

In the case of intersubband excitations $|n\rangle \rightarrow |m\rangle$ there are two different types of transitions as indicated by Fig. 4. The first type ends at a subband which is not occupied. For wave vectors small compared to the Fermi wave vector of the starting level, these transitions have a full linewidth of $2\hbar q v_{F,n}$ and are centered at the subband spacing $E_{nm} = E_n - E_m$ [Fig. 4(b)]. If the upper level is partially occupied, some transitions close the subband spacing are forbidden because of the Pauli exclusion principle. This forbidden region becomes larger with increasing occupation of the upper level. The result is a splitting of the intersubband excitation into two peaks [Fig. 4(c)]. An evaluation of the line shape by summing up all intersubband contributions within a harmonic oscillator model, using the same parameters as in the case of intrasubband excitations, is shown in Fig. 3 for different wave vectors $q_\parallel$ (solid line). We obtain one peak centered at the $\Delta n = 2$ intersubband spacing. The linewidth of this peak is essentially determined by the Fermi velocity of the lowest subband and in good agreement with the experiment. However, this model does not describe the intensity dip observed for large wave vectors $q_\parallel$. The dashed line in Fig. 3 shows the calculated intersubband line shape if transitions that end in

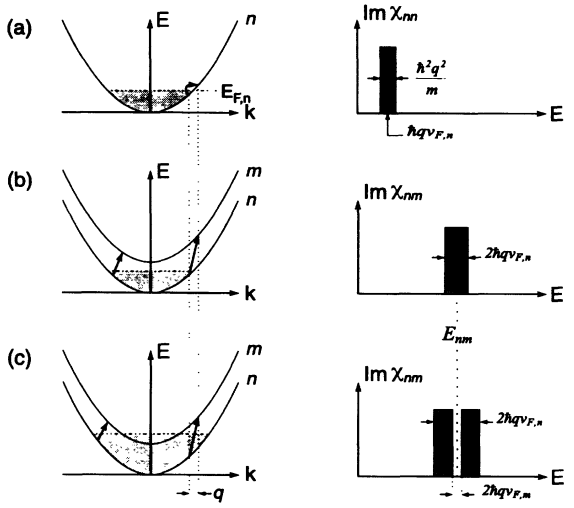

FIG. 4. Schematic sketch of different one-dimensional single-particle transitions and imaginary parts of their corresponding polarizabilities for $T = 0$ K and infinite scattering time. (a) Describes intrasubband excitations $|n\rangle \rightarrow |n\rangle$; (b) and (c) show intersubband transitions $|n\rangle \rightarrow |m\rangle$ for empty and occupied levels $|m\rangle$, respectively.

unoccupied levels are neglected. Since the initial levels of these transitions are only weakly occupied, they contribute predominantly at the center of the intersubband peak within a purely parabolic model potential. Neglecting them accounts for an increasing intensity dip in the center of the intersubband peak with increasing wave vector $q_{\|}$. Both models lead to a linewidth of the excitation which is correlated to the energetic position of the intrasubband excitations and given by $2\hbar q v_F$, which exceeds the linewidth induced by inhomogenous broadening for wave vectors larger than 7×10^4 cm^{-1} in our sample. The experimental observation of an intensity dip for large wave vectors suggests that those transitions that end in unoccupied levels are slightly redshifted. This effect can be due to a reduction of the subband spacing for empty levels which are already close to the maximum of the lateral potential. The occurrence of the intensity dip is not only a characteristic signature for single-particle behavior but also for a deviation from a strict harmonic oscillator potential. Goñi *et al.* pointed out the existence of such an intersubband single-particle gap by studying intersubband plasmons within this gap [3]. This excitation was observed to be essentially free from Landau damping for sufficiently large wave vectors. This shows that either the coupling of the plasmon to the SPE in the gap is weak or their potential shape reveals deviations from a harmonic oscillator potential at high energies similar to the present case.

In conclusion, we have observed interlevel excitations in zero-dimensional systems by resonant inelastic light scattering. Increasing confinement energies for decreasing structure size as well as nondispersive behavior have been demonstrated. In quantum wire structures, the wave vector dispersion of intersubband and intrasubband excitations has been measured. The systematic variation of the transitions in energy and shape are explained theoretically, considering single-particle excitations in quantum wires with several occupied subbands.

We want to thank T. Egeler and P. Baumgartner for many discussions and M. Holzmann for supplementary magnetotransport measurements. This work is financially supported by the Deutsche Forschungsgemeinschaft via SFB 348.

[1] For a review, see A. Pinczuk and G. Abstreiter, in *Light Scattering in Solids V,* edited by M. Cardona and G. Güntherodt (Springer-Verlag, Berlin, 1989), p. 5.

[2] A. Pinczuk, D. Heiman, S. Schmitt-Rink, C. Kallin, B. S. Dennis, L. N. Pfeiffer, and K. W. West, in *Light Scattering in Semiconductor Structures and Superlattices,* edited by D. J. Lockwood and J. F. Young (Plenum Press, New York, 1991), p. 571.

[3] A. R. Goñi, A. Pinczuk, J. S. Weiner, J. M. Calleja, B. S. Dennis, L. N. Pfeiffer, and K. W. West, Phys. Rev. Lett. **67**, 3298 (1991); see also, A. R. Goñi *et al.,* in *Phonons in Semiconductor Nanostructures,* edited by J.-P. Leburton, J. Pascual, and C. Sotomayor Torres, NATO Advanced Study Institutes, Ser. E, Vol. 236 (Kluwer Academic, Dordrecht, 1993), p. 287.

[4] A. Schmeller, A. R. Goñi, A. Pinczuk, J. M. Calleja, B. S. Dennis, L. N. Pfeiffer, and K. W. West, Solid State Electron. **37**, 1281 (1994).

[5] A. Schmeller, A. R. Goñi, A. Pinczuk, J. S. Weiner, J. M. Calleja, B. S. Dennis, L. N. Pfeiffer, and K. W. West, Phys. Rev. B **49**, 14 778 (1994).

[6] T. Egeler, G. Abstreiter, G. Weimann, T. Demel, D. Heitmann, P. Grambow, and W. Schlapp, Phys. Rev. Lett. **65**, 1804 (1990).

[7] P. W. Park, A. H. MacDonald, and W. L. Schaich, Phys. Rev. B **46**, 12 635 (1992).

[8] R. Decca, A. Pinczuk, S. Das Sarma, B. S. Dennis, L. N. Pfeiffer, and K. W. West, Phys. Rev. Lett. **72**, 1506 (1994).

[9] P. I. Tamborenea and S. Das Sarma, Phys. Rev. B **49**, 16 821 (1994).

[10] J. S. Weiner, G. Danan, A. Pinczuk, J. Valladares, L. N. Pfeiffer, and K. West, Phys. Rev. Lett. **63**, 1641 (1989).

[11] F. Hirler, R. Strenz, R. Küchler, G. Abstreiter, G. Böhm, J. Smoliner, G. Tränkle, and G. Weimann, Semicond. Sci. Technol. **8**, 617 (1993).

[12] R. Strenz, V. Roβkopf, F. Hirler, G. Abstreiter, G. Böhm, G. Tränkle, and G. Weimann, Semicond. Sci. Technol. **9**, 399 (1994).

[13] G. Fasol, N. Mestres, M. Dobers, A. Fischer, and K. Ploog, Phys. Rev. B **36**, 1565 (1987).

[14] David A. Dahl and L. J. Sham, Phys. Rev. B **16**, 651 (1977).

[15] Q. P. Li and S. Das Sarma, Phys. Rev. B **43**, 11 768 (1991).

[16] K.-F. Berggren, G. Roos, and H. van Houten, Phys. Rev. B **37**, 10 118 (1988).

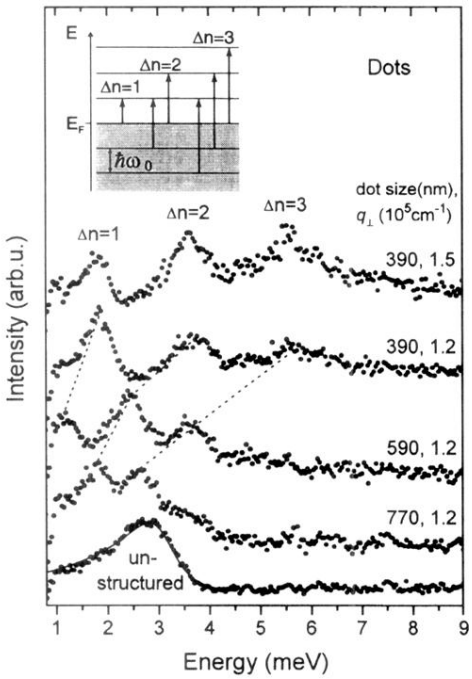

FIG. 1. Depolarized light scattering by interlevel excitations in quantum dots. The two parameters at each spectrum denote the geometrical dot size and wave vector. The lowest spectrum shows the reference measurement of the as-grown sample and a line shape fit (continuous line). All contributing transitions are schematically shown in the inset.

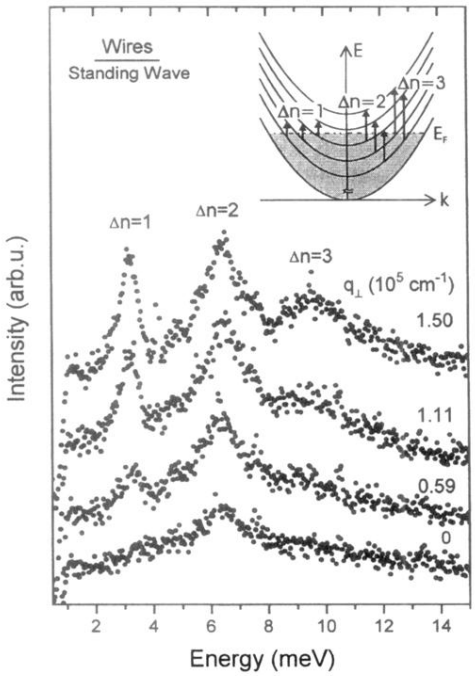

FIG. 2. Depolarized light scattering spectra of a wire sample mounted in standing wave geometry for different wave vectors $q_\perp$. The inset schematically shows intersubband excitations of different orders for $q_\parallel = 0$.

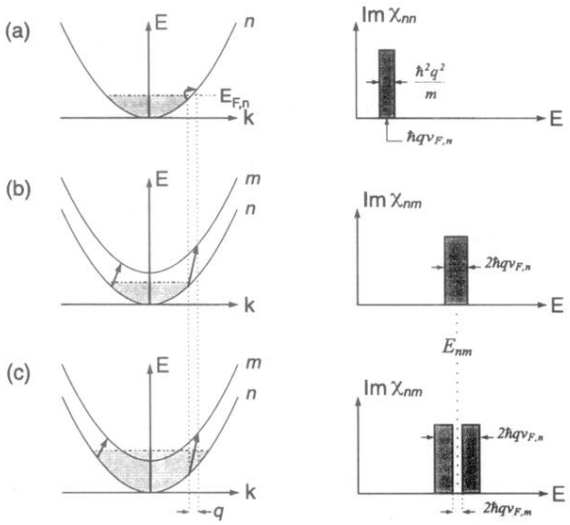

FIG. 4. Schematic sketch of different one-dimensional single-particle transitions and imaginary parts of their corresponding polarizabilities for $T = 0$ K and infinite scattering time. (a) Describes intrasubband excitations $|n\rangle \rightarrow |n\rangle$; (b) and (c) show intersubband transitions $|n\rangle \rightarrow |m\rangle$ for empty and occupied levels $|m\rangle$, respectively.